AIAA 2000-3191

Improved Mean-Flow Solution for Slab Rocket Motors with Regressing Walls

Chong Zhou and Joseph Majdalani
Marquette University
Milwaukee, WI 53233

36th AIAA/ASME/SAE/ASEE
Joint Propulsion Conference
16–19 July 2000, Huntsville, AL

Improved Mean-Flow Solution for Slab Rocket Motors with Regressing Walls

C. Zhou* and J. Majdalani†
Marquette University, Milwaukee, WI 53233

The Navier-Stokes equations are solved to obtain an exact description of the internal mean flow in a slab rocket motor having a rectangular cross section and two equally regressing porous walls. The scope is limited to two-dimensional incompressible and nonreactive laminar flow. In seeking an exact solution, similarity transformations are used in both space and time. Subsequently, the original problem is reduced to a single fourth-order differential equation with four boundary conditions. The exact similarity transformations involve a linearly varying axial velocity, an axially independent normal velocity, and a constant dimensionless regression ratio. The emerging nonlinear differential equation is solved both numerically and asymptotically, using regular perturbations in the injection Reynolds number *R*. Results are correlated and compared via variations in *R* and the dimensionless wall regression rate α. For hard blowing and moderate regression rates, the effect of varying α is found to be small. This justifies the use of Taylor's mean-flow profile in high Reynolds number applications. For small regression rates, the agreement between analytical and numerical solutions appears to be quite satisfactory. Since most physical problems correspond to small values of α, the analytical solution constitutes a practical equivalent to the numerical solution over a wide range of *R*. By way of verification, the governing equation we obtain is reducible to the classic Berman equation when regression is suppressed. Moreover, the asymptotic solution reduces to Taylor's classic expression for large injection. From the analytical formulation, closed-form expressions are produced for the velocity, pressure and shear stress distributions.

I. Introduction

MATHEMATICAL flow models of the internal gas dynamics in solid rocket motors have relied on subdividing the field into a mean and a time-dependent component. Recent analyses by Flandro,[1-3] Majdalani,[4,5] and Majdalani and Van Moorhem[6,7] have been successful in producing time-dependent solutions that could incorporate both viscous and rotational effects. At the outset, both viscous and rotational effects were shown to play important roles in prescribing the temporal flow behavior. In most of these studies, the mean-flow profile was based on Culick's inviscid solution[8] which coincided with Taylor's[9] and Yuan's[10] independently derived expressions for infinitely large injection.

Culick's profile given in 1966 was a definite improvement over the one-dimensional potential flow approximation that was being used, at the time, for the circular-grain motor. Unlike its predecessor, Culick's approximation was more capable of mimicking the burning process. In addition to satisfying the no flow through the head end, Culick's solution[8] included the effects of boundary-driven vorticity and employed a uniform speed that was normal to the burning surface. Despite its omission of viscosity and grain regression, Culick's mean flow was shown to be surprisingly adequate both in numerical[11-13] and experimental[14-16] simulations of the hard-blowing process at the porous walls. However, for moderate cross-flow Reynolds numbers or fast regression rates, there may be occasions when more precise information is required. Also, since the mean-flow expressions must be fed into the time-dependent formulations, it would be desirable to retain viscous and rotational effects in both mean and unsteady components of the flow. In that spirit, the current article will focus on presenting a rotational mean-flow solution that incorporates both viscosity and the effects of wall regression. The outcome should be a field that is consistently rotational and viscous in both its mean and time-dependent components. The geometry that will be considered is that of the slab

*Graduate Research Assistant. Student Member AIAA.
†Assistant Professor, Department of Mechanical and Industrial Engineering. Member AIAA.

rocket motor. This will be idealized as a long and slender channel with regressing walls.

The method to be utilized is as follows: The Navier-Stokes equations will be first reduced to one exact, fourth-order, nonlinear differential equation whose solution is prescribed by four boundary conditions. The approach follows similarity transformations in both space and time that evolve from the works of Berman,[17] Yuan and Finkelstein,[18] and Goto and Uchida.[19] The spatial transformations take advantage of flow similarity by presuming a linearly varying axial velocity, and a normal velocity that is independent of the axial coordinate. The temporal transformation assumes a constant dimensionless expansion ratio. As such, the chamber expands uniformly from the symmetry plane and the injected flow enters the chamber uniformly across, and normal to, the porous walls. Under these conditions, the two-dimensional Navier-Stokes equations collapse into a single nonlinear differential equation that can be solved both numerically and asymptotically.

The equation obtained will be shown to reduce to the classic Berman form[17] when the porous walls are made motionless. Additionally, the asymptotic solution that is constructed using regular perturbations in the injection Reynolds number will be shown to reduce to Taylor's[9] or Yuan's[10] for large injection in porous channels with stationary walls. From the asymptotic solution, closed-form expressions will be obtained for the velocity, pressure and shear stress at the wall. These will be used to characterize the flow. Furthermore, comparisons with the numerical solution will demonstrate the accuracy of the analytical formulations over a wide range of moderate-to-high Reynolds numbers. For high Reynolds numbers, the effect of varying the expansion rate will be shown to have little effect on the solution. Overall, the solutions precipitated from this study are hoped to improve our understanding of laminar flows in porous channels and tubes. In particular, the enhanced models are hoped to be later substituted into the temporal field expressions, and then implemented into the known Standard Stability Program (SSP).[20,21]

II. Mathematical Model

The slab rocket motor is modeled as a channel of rectangular cross section. One side of the cross section, representing the distance ($2a$) between the porous walls is taken to be smaller than the other two. This enables us to treat the problem as a case of two-dimensional flow. Both sidewalls are assumed to have equal permeability and to expand uniformly at a time-dependent rate $\dot{a}$. Inasmuch as the forthcoming similarity solution obviates the need to specify a finite body length L, one has the liberty to assume a semi-infinite length.[22] In order to accommodate expanding

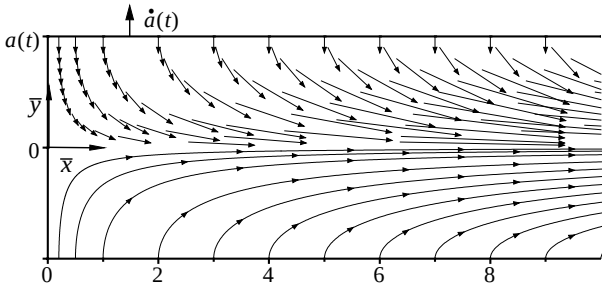

Fig. 1 Coordinate system and bulk fluid motion.

boundaries, the head end is closed by a compliant membrane which is allowed to stretch with channel expansion.

As shown in Fig. 1, a coordinate system may be chosen with the origin at the center of the channel. Using the over-bar to denote dimensional variables, we use $\overline{x}$ and $\overline{y}$ to define the axial and normal coordinates. The corresponding axial and normal velocity components are defined as $\overline{u}$ and $\overline{v}$, respectively. For even wall injection and no flow across the midsection plane, symmetry can identified at $\overline{y} = 0$. Thus it is sufficient to limit the investigation over half the channel, extending from the midplane to the wall, $0 \le \overline{y} \le a$.

For two-dimensional laminar and incompressible flow with no body forces, the differential expressions for mass and momentum conservation can be written as

$$\frac{\partial \overline{u}}{\partial \overline{x}} + \frac{\partial \overline{v}}{\partial \overline{y}} = 0 \tag{1}$$

$$\frac{\partial \overline{u}}{\partial t} + \overline{u}\frac{\partial \overline{u}}{\partial \overline{x}} + \overline{v}\frac{\partial \overline{u}}{\partial \overline{y}} = -\frac{1}{\rho}\frac{\partial \overline{p}}{\partial \overline{x}} + \nu\left(\frac{\partial^2 \overline{u}}{\partial \overline{x}^2} + \frac{\partial^2 \overline{u}}{\partial \overline{y}^2}\right) \tag{2}$$

$$\frac{\partial \overline{v}}{\partial t} + \overline{u}\frac{\partial \overline{v}}{\partial \overline{x}} + \overline{v}\frac{\partial \overline{v}}{\partial \overline{y}} = -\frac{1}{\rho}\frac{\partial \overline{p}}{\partial \overline{y}} + \nu\left(\frac{\partial^2 \overline{v}}{\partial \overline{x}^2} + \frac{\partial^2 \overline{v}}{\partial \overline{y}^2}\right) \tag{3}$$

where ρ, $\overline{p}$, ν, and t are the dimensional density, pressure, kinematic viscosity, and time. The boundary conditions are:

$$\overline{u}(\overline{x}, a) = 0 \qquad \overline{v}(a) = v_w = -A\dot{a} \tag{4}$$

$$\frac{\partial \overline{u}}{\partial \overline{y}}(\overline{x}, 0) = 0 \qquad \overline{v}(0) = 0 \tag{5}$$

$$\overline{u}(0, \overline{y}) = 0\,. \tag{6}$$

At the wall, it is assumed that the fluid inflow velocity v_w is independent of position. Additionally, the injection coefficient ($A \equiv -v_w / \dot{a}$) that appears in Eq. (4) is a measure of wall porosity. For example, in the absence of forced injection (e.g., for nonreactive walls), one may use $A = 1$. That case would correspond to an

expansion process that allows the fluid to be admitted into the chamber at a speed that is exactly equal to the rate of regression $-\dot{a}$ (see Eq. (4)).

By applying mass conservation to a volume of fluid V extending from $\overline{x}=0$ to an arbitrary $\overline{x}$, the average flow velocity $\overline{u}_{\mathrm{m}}$ can be determined at any position to be

$$\overline{u}_{\mathrm{m}}(\overline{x})=\frac{1}{S}\int_{S}\vec{u}\cdot\mathrm{d}\vec{S}\,, \tag{7}$$

where S is the surface area of the cross section at any location $\overline{x}$. The corresponding average mass flow rate can be calculated from integration over the control volume

$$\dot{\overline{m}}_{\mathrm{m}}=\rho S\overline{u}_{\mathrm{m}}=\frac{\partial}{\partial t}\int_{V}\rho\,\mathrm{d}V\,, \tag{8}$$

where $\mathrm{d}V=S\,\mathrm{d}\overline{x}$. By substituting Eq. (7) into Eq. (8), one gets

$$a\overline{u}_{\mathrm{m}}=\frac{\partial}{\partial t}(a\overline{x}),\qquad \overline{u}_{\mathrm{m}}=-\frac{\dot{a}\overline{x}}{a}\,. \tag{9}$$

At this point, the Stokes stream function can be introduced. This allows replacing the two velocity components by one single variable. This may be accomplished via

$$\overline{u}=\frac{\partial\overline{\psi}}{\partial\overline{y}}\,,\quad \overline{v}=-\frac{\partial\overline{\psi}}{\partial\overline{x}}\,. \tag{10}$$

Following this transformation, the number of dependent variables is reduced by one. The number of equations is also reduced by one since the continuity equation becomes redundant to $\overline{\psi}$.

Pressure can also be eliminated from the momentum equation by transforming it into the vorticity transport equation. This can be accomplished by taking the curl of the momentum equation. This operation eliminates the pressure from the momentum equation and introduces, in its stead, the flow vorticity. Thus,

$$\nabla\times\left(\frac{\mathrm{D}\vec{V}}{\mathrm{D}t}=-\frac{1}{\rho}\nabla\overline{p}+\nu\nabla^{2}\vec{V}\right) \tag{11}$$

gives $$\frac{\partial\overline{\zeta}}{\partial t}+\overline{u}\frac{\partial\overline{\zeta}}{\partial\overline{x}}+\overline{v}\frac{\partial\overline{\zeta}}{\partial\overline{y}}=\nu\left(\frac{\partial^{2}\overline{\zeta}}{\partial\overline{x}^{2}}+\frac{\partial^{2}\overline{\zeta}}{\partial\overline{y}^{2}}\right), \tag{12}$$

where

$$\overline{\zeta}=\frac{\partial\overline{v}}{\partial\overline{x}}-\frac{\partial\overline{u}}{\partial\overline{y}}\,. \tag{13}$$

III. Reduction of the Flow Equations

A. Similar Solution in Space

A similar solution with respect to $\overline{x}$ can be developed from mass conservation. In fact, a simple mass balance suggests that $\overline{v}/\overline{u}=\overline{x}/a$. Following Berman's classic approach, and in view of the boundary conditions given by Eqs. (4) and (5), a similar solution can be developed from the mean-flow stream function. Defining the dimensionless normal coordinate to be

$$y=\overline{y}/a\,, \tag{14}$$

the stream function can be written as

$$\overline{\psi}=\nu h(a)\overline{x}\overline{F}(y,t) \tag{15}$$

where $\overline{F}(y,t)$ is independent of the axial coordinate, and $h(a)$ is some subsidiary function. Inserting Eq. (15) into Eq. (10), the axial and normal velocities can be expressed as

$$\overline{u}=\frac{\nu\overline{x}}{a}h(a)\overline{F}_{y}\,,\text{ and }\ \overline{v}=-\nu h(a)\overline{F}(y,t)\,, \tag{16}$$

where $\overline{F}_{y}=\partial\overline{F}/\partial y$. Due to the linear spatial dependence, we have

$$\overline{u}_{\overline{xx}}=\overline{v}_{\overline{x}}=0\,. \tag{17}$$

As $\overline{v}$ is independent of $\overline{x}$, the vorticity equation simply becomes

$$\overline{\zeta}=-\frac{\partial\overline{u}}{\partial\overline{y}} \tag{18}$$

whereby Eq. (3) reduces to $\overline{p}_{\overline{yx}}=0$. Upon substitution into Eq. (12) (i.e., the vorticity transport equation), one obtains

$$\overline{u}_{\overline{y}t}+\overline{u}\overline{u}_{\overline{yx}}+\overline{v}\overline{u}_{\overline{yy}}=\nu\overline{u}_{\overline{yyy}}\,. \tag{19}$$

Plugging Eq. (16) into Eq. (19) gives

$$\left[\frac{\nu\overline{x}}{a^{2}}h(a)\overline{F}_{\overline{yy}}\right]_{t}+\frac{\nu^{2}\overline{x}}{a^{3}}h^{2}(a)\overline{F}_{\overline{y}}\overline{F}_{\overline{yy}}$$

$$-\frac{\nu^2\overline{x}}{a^3}h^2(a)\overline{F}\overline{F}_{\overline{yyy}} = \frac{\nu^2\overline{x}}{a^4}h(a)\overline{F}_{\overline{yyyy}}\,. \tag{20}$$

This equation will be dimensionally homogeneous if, and only if

$$\frac{\nu^2\overline{x}}{a^3}h^2(a) \sim \frac{\nu^2\overline{x}}{a^4}h(a)\,. \tag{21}$$

Therefore, without loss in generality, one must have

$$h(a) = a^{-1}\,. \tag{22}$$

With this realization, the dimensional axial and normal velocities can be written as

$$\overline{u} = \frac{\nu\overline{x}}{a^2}\overline{F}_y\,, \quad \text{and} \quad \overline{v} = -\frac{\nu}{a}\overline{F}(y,t)\,. \tag{23}$$

B. Transformed Equation

In order to solve Eq. (19), one must start by evaluating its partial derivatives. For example, by applying the chain rule to Eq. (23) we obtain

$$\overline{u}_{\overline{y}} = \left(\frac{\nu\overline{x}}{a^2}\overline{F}_y\right)_{\overline{y}} = \left(\frac{\nu\overline{x}}{a^2}\overline{F}_y\right)_y\frac{\partial y}{\partial\overline{y}}\,. \tag{24}$$

Using $y = \overline{y}/a$, Eq. (24) becomes

$$\overline{u}_{\overline{y}} = \frac{1}{a}\left(\frac{\nu\overline{x}}{a^2}\overline{F}_y\right)_y = \frac{\nu\overline{x}}{a^3}\overline{F}_{yy}\,. \tag{25}$$

In turn, partial derivatives change into

$$\overline{u}_{\overline{yx}} = \left(\frac{\nu\overline{x}}{a^3}\overline{F}_{yy}\right)_{\overline{x}} = \frac{\nu}{a^3}\overline{F}_{yy}\,, \tag{26}$$

$$\overline{u}_{\overline{yy}} = \left(\frac{\nu\overline{x}}{a^3}\overline{F}_{yy}\right)_{\overline{y}} = \frac{\nu\overline{x}}{a^4}\overline{F}_{yyy}\,, \tag{27}$$

$$\overline{u}_{\overline{yyy}} = \left(\frac{\nu\overline{x}}{a^4}\overline{F}_{yyy}\right)_{\overline{y}} = \frac{\nu\overline{x}}{a^5}\overline{F}_{yyyy}\,. \tag{28}$$

Recalling that y and a are time-dependent, one may evaluate $\overline{u}_{\overline{yt}}$ as

$$\overline{u}_{\overline{yt}} = \left(\frac{\nu\overline{x}}{a^3}\overline{F}_{yy}\right)_t = \frac{\nu\overline{x}}{a^3}\overline{F}_{yyt} + \frac{\nu\overline{x}}{a^3}\overline{F}_{yyy}\frac{\partial y}{\partial t} - \frac{3\nu\overline{x}\dot{a}}{a^4}\overline{F}_{yy} \tag{29}$$

where

$$\frac{\mathrm{d}y}{\mathrm{d}t} = -\frac{\dot{a}y}{a}\,. \tag{30}$$

Collecting terms, we arrive at

$$\overline{u}_{\overline{yt}} = \frac{\nu\overline{x}}{a^3}\overline{F}_{yyt} - \frac{\nu\overline{x}\dot{a}}{a^4}y\overline{F}_{yyy} - \frac{3\nu\overline{x}\dot{a}}{a^4}\overline{F}_{yy}\,. \tag{31}$$

By substituting Eqs. (26)–(28), and Eq. (31) into Eq. (19), a differential equation is developed for $\overline{F}$. This is

$$\overline{F}_{yyyy} + \alpha\left(y\overline{F}_{yyy} + 3\overline{F}_{yy}\right) + \overline{F}\overline{F}_{yyy} - \overline{F}_y\overline{F}_{yy} - a^2\nu^{-1}\overline{F}_{yyt} = 0\,. \tag{32}$$

where α is the wall regression ratio defined by

$$\alpha = \frac{\dot{a}a}{\nu}\,. \tag{33}$$

Note that the regression ratio will be positive for expanding walls. A careful integration of Eq. (32) produces

$$\left[\overline{F}_{yyy} + \alpha\left(y\overline{F}_{yy} + 2\overline{F}_y\right) + \overline{F}\overline{F}_{yy} - \left(\overline{F}_y\right)^2 - a^2\nu^{-1}\overline{F}_{yt}\right] = \lambda\,, \tag{34}$$

where λ is a constant. The boundary conditions given by Eqs. (4)–(5) can be updated into

$$\begin{aligned} \overline{F}_{yy}(0) &= 0 & \overline{F}(0) &= 0 \\ \overline{F}_y(1) &= 0 & \overline{F}(1) &= R \end{aligned} \tag{35}$$

where R is the injection Reynolds number defined by

$$R = a v_{\mathrm{w}}/\nu\,. \tag{36}$$

Quantities expressed by Eqs. (15), (23), (32) and (35) can be normalized via

$$\psi = \frac{\overline{\psi}}{a v_w},\ u = \frac{\overline{u}}{v_w},\ v = \frac{\overline{v}}{v_w},\ x = \frac{\overline{x}}{a},\ F = \frac{\overline{F}}{R} \tag{37}$$

where F is the characteristic mean-flow function. When this dimensionless set is used, the normalized equations become

$$\psi = xF \tag{38}$$

$$u = xF_y\,, \qquad v = -F \tag{39}$$

$$u_{\mathrm{m}} = -x\dot{a}/v_{\mathrm{w}} = x/A \tag{40}$$

$$R^{-1}F_{yyyy} + \alpha R^{-1}\left(yF_{yyy} + 3F_{yy}\right) + FF_{yyy}$$

$$-F_y F_{yy} - a^2 R^{-1} \nu^{-1} F_{yyt} = 0 \tag{41}$$

and, finally,

$$F_{yy}(0) = 0\,,\ F(0) = 0\,,\ F_y(1) = 0\,,\ F(1) = 1\,. \tag{42}$$

C. Similar Solution in Space and Time

A similar solution with respect to space and time can now be developed. For constant α and $F = F(y)$, it follows that $F_{yyt} = 0$. To realize this condition, the value of the regression ratio α must be specified by its initial value

$$\alpha = \frac{\dot{a} a}{\nu} = \frac{\dot{a}_0 a_0}{\nu}\,, \tag{43}$$

where a_0 and $\dot{a}_0$ denote the initial channel height and regression rate. The temporal similarity transformation can be achieved by integrating Eq. (43) with respect to time. Forthwith, a similar solution for the temporal channel height is produced. This is

$$a(t) = a_0 \sqrt{1 + 2\nu\alpha t a_0^{-2}}\,. \tag{44}$$

From Eq. (4), an expression for the injection velocity variation can be determined, provided that the injection coefficient A in Eq. (4) is constant:

$$\frac{\dot{a}(t)}{\dot{a}_0} = \frac{v_{\mathrm{w}}(t)}{v_{\mathrm{w}}(0)} = \left(1 + \frac{2\nu\alpha t}{a_0^2}\right)^{-\frac{1}{2}} \cong 1 - \frac{\nu\alpha t}{a_0^2}\,. \tag{45}$$

Under these provisions, Eq. (41) becomes

$$R^{-1} F^{IV} + \alpha R^{-1}\left(yF''' + 3F''\right) + FF''' - F'F'' = 0 \tag{46}$$

where a prime denotes differentiation with respect to y. The exact solution of the problem becomes contingent upon finding an F that satisfies

$$F''(0) = 0\,,\ F(0) = 0\,,\ F'(1) = 0\,,\ F(1) = 1. \tag{47}$$

Note that Berman's classic equation[17] is a special case of Eq. (46) that can be obtained by suppressing α.

IV. Analytical Solution

For moderate-to-large values of the Reynolds number, Eq. (46) can be solved asymptotically. For that purpose, we define $\varepsilon \equiv R^{-1}$ as our perturbation parameter. The problem becomes that of solving

$$\varepsilon F^{IV} + \alpha\varepsilon\left(yF''' + 3F''\right) + FF''' - F'F'' = 0\,. \tag{48}$$

where a small parameter multiplies the highest derivative. Evidently, a regular perturbation expansion of the form $F = F_0 + \varepsilon F_1 + O(\varepsilon^2)$ can be attempted.

Substitution into Eq. (48) gives, at $O(1)$

$$F_0 F_0''' - F_0' F_0'' = 0\,, \tag{49}$$

with $F_0'(1) = 0,\ F_0(1) = 1,\ F_0(0) = 0$. It can be easily verified that the leading-order solution is $F_0 = \sin\theta$, where $\theta = \frac{1}{2}\pi y$.

A. First-order Equation

Terms of $O(\varepsilon)$ can be gathered and separated. The emerging first-order equation is

$$\begin{aligned} &F_0 F_1''' - F_0' F_1'' - F_0'' F_1' + F_0''' F_1 \\ &\quad = -F_0^{IV} - 3\alpha F_0'' - \alpha y F_0'''\,. \end{aligned} \tag{50}$$

This needs to be solved while satisfying

$$F_1'(1) = 0,\ F_1(1) = 0,\ F_1(0) = 0\,. \tag{51}$$

Switching to θ as the independent variable, and using $F_0 = \sin\theta$, Eq. (50) becomes

$$\begin{aligned} &\sin\theta F_1''' - \cos\theta F_1'' + \sin\theta F_1' - \cos\theta F_1 \\ &\quad = (6\alpha/\pi - \tfrac{1}{2}\pi)\sin\theta + (2\alpha/\pi)\theta\cos\theta\,, \end{aligned} \tag{52}$$

$$\text{with} \qquad F_1'\left(\tfrac{1}{2}\pi\right) = 0,\ F_1\left(\tfrac{1}{2}\pi\right) = 0,\ F_1(0) = 0\,. \tag{53}$$

B. Solving by Variation of Parameters

The solution of Eq. (52) must be carefully constructed. First, one can attempt to solve the homogeneous equation,

$$\sin\theta F_1''' - \cos\theta F_1'' + \sin\theta F_1' - \cos\theta F_1 = 0\,. \tag{54}$$

To that end, one simple solution exhibited by Eq. (54) can be guessed to be

$$F_{1h} = \cos\theta\,. \tag{55}$$

Having determined one independent solution, the method of variation of parameters may be employed. This requires setting

$$F_{1H} = C(\theta)\cos\theta \tag{56}$$

where $C(\theta)$ is unknown. Differentiation gives

$$F'_{1H} = C'\cos\theta - C\sin\theta\,, \tag{57}$$
$$F''_{1H} = C''\cos\theta - 2C'\sin\theta - C\cos\theta\,, \tag{58}$$
$$F'''_{1H} = C'''\cos\theta - 3C''\sin\theta - 3C'\cos\theta + C\sin\theta\,. \tag{59}$$

Substitution into Eq. (54) yields

$$C'''\sin\theta\cos\theta - 2C''\sin^2\theta - C'' = 0\,. \tag{60}$$

Thus C can be determined to be

$$C(\theta) = K_0\tan\theta + K_1\theta + K_2\,, \tag{61}$$

where K_0, K_1, and K_2 are integration parameters. This completes the expression for the general homogeneous solution

$$F_{1H} = K_0\sin\theta + K_1\theta\cos\theta + K_2\cos\theta\,. \tag{62}$$

According to the method of variation of parameters, the three constants K_0, K_1, and K_2 must be allowed to vary with θ. At the outset, Eq. (62) becomes

$$\begin{aligned} F_1(\theta) &= K_0(\theta)\sin\theta + K_1(\theta)\theta\cos\theta + K_2(\theta)\cos\theta \\ &\equiv K_0(\theta)F_{1A}(\theta) + K_1(\theta)F_{1B}(\theta) + K_2(\theta)F_{1C}(\theta)\,. \end{aligned} \tag{63}$$

This term needs to be differentiated three times before substitution into Eq. (52). The first differentiation yields

$$\begin{aligned} F'_1 = {} & K'_0F_{1A} + K_0F'_{1A} + K'_1F_{1B} + K_1F'_{1B} \\ & + K'_2F_{1C} + K_2F'_{1C}\,. \end{aligned} \tag{64}$$

A procedural constraint binding the derivatives of the varying parameters is $K'_0F_{1A} + K'_1F_{1B} + K'_2F_{1C} = 0$. Hence, by virtue of

$$K'_0\sin\theta + K'_1\theta\cos\theta + K'_2\cos\theta = 0\,, \tag{65}$$

Eq. (64) becomes

$$\begin{aligned} F'_1 = {} & K_0F'_{1A} + K_1F'_{1B} + K_2F'_{1C} \\ = {} & K_0\cos\theta + K_1(\cos\theta - \theta\sin\theta) - K_2\sin\theta\,. \end{aligned} \tag{66}$$

Differentiating a second time renders

$$\begin{aligned} F''_1 = {} & K'_0F'_{1A} + K_0F''_{1A} + K'_1F'_{1B} + K_1F''_{1B} \\ & + K'_2F'_{1C} + K_2F''_{1C}\,. \end{aligned} \tag{67}$$

Similarly, letting $K'_0F'_{1A} + K'_1F'_{1B} + K'_2F'_{1C} = 0$ gives

$$K'_0\cos\theta + K'_1(\cos\theta - \theta\sin\theta) - K'_2\sin\theta = 0\,. \tag{68}$$

Equation (67) becomes

$$\begin{aligned} F''_1 = {} & K_0F''_{1A} + K_1F''_{1B} + K_2F''_{1C} = -K_0\sin\theta \\ & - K_1(2\sin\theta + \theta\cos\theta) - K_2\cos\theta\,. \end{aligned} \tag{69}$$

Finally, differentiating a third time brings about

$$\begin{aligned} F'''_1 = {} & -K'_0\sin\theta - K_0\cos\theta - K'_1(2\sin\theta + \theta\cos\theta) \\ & - K_1(3\cos\theta - \theta\sin\theta) - K'_2\cos\theta + K_2\sin\theta\,. \end{aligned} \tag{70}$$

We now substitute F_1 and its derivatives, given by Eqs. (63), (66), (69), and (70), back into the complete first-order equation, given by Eq. (52). The result is

$$\begin{aligned} & -K'_0\sin^2\theta - 2K'_1\sin^2\theta - K'_1\theta\sin\theta\cos\theta \\ & - K'_2\sin\theta\cos\theta = \left(\frac{6\alpha}{\pi} - \frac{\pi}{2}\right)\sin\theta + \frac{2\alpha}{\pi}\theta\cos\theta\,. \end{aligned} \tag{71}$$

Equation (71) contains three unspecified functions, K'_0, K'_1, and K'_2. In order to obtain closure, the two constraints introduced in Eqs. (65) and (68) must be employed alongside Eq. (71). The solution is

$$K'_0(\theta) = \frac{\alpha\theta\cos^3\theta}{\pi\sin^2\theta} - \left(\frac{\pi}{4} - \frac{3\alpha}{\pi}\right)\frac{\cos^2\theta}{\sin\theta} \tag{72}$$

$$K'_1(\theta) = \left(\frac{\pi}{4} - \frac{3\alpha}{\pi}\right)\frac{1}{\sin\theta} - \frac{\alpha\theta\cos\theta}{\pi\sin^2\theta} \tag{73}$$

$$\begin{aligned} K'_2(\theta) = {} & \left(\frac{\pi}{4} - \frac{3\alpha}{\pi}\right)\left(\cos\theta - \frac{\theta}{\sin\theta}\right) \\ & - \frac{\alpha\theta\cos^2\theta}{\pi\sin\theta} + \frac{\alpha\theta^2\cos\theta}{\pi\sin^2\theta}\,. \end{aligned} \tag{74}$$

Integrating for the variable parameters, one obtains

$$\begin{aligned} K_0(\theta) = {} & -\frac{\alpha}{\pi}\left(\frac{\theta}{\sin\theta} + \theta\sin\theta\right) + \left(\frac{2\alpha}{\pi} - \frac{\pi}{4}\right)\cos\theta \\ & + \left(\frac{4\alpha}{\pi} - \frac{\pi}{4}\right)\ln\tan\frac{\theta}{2} + c_0 \end{aligned} \tag{75}$$

$$K_1(\theta) = \left(\frac{\pi}{4} - \frac{4\alpha}{\pi}\right)\ln\tan\frac{\theta}{2} + \frac{\alpha}{\pi}\frac{\theta}{\sin\theta} + c_1 \tag{76}$$

$$K_2(\theta) = \left(\frac{\pi}{4} - \frac{2\alpha}{\pi}\right)\sin\theta - \frac{\alpha}{\pi}\left(\theta\cos\theta + \frac{\theta^2}{\sin\theta}\right) + \left(\frac{4\alpha}{\pi} - \frac{\pi}{4}\right)S(\theta) + c_2\,, \tag{77}$$

where c_0, c_1, and c_2 are constants and

$$S(\theta) \equiv \int_0^\theta \phi\csc\phi\,\mathrm{d}\phi\,. \tag{78}$$

Inserting Eqs. (75)–(77) into Eq. (63) yields

$$F_1 = -\frac{2\alpha}{\pi}\theta + \left(\frac{4\alpha}{\pi} - \frac{\pi}{4}\right)\left[(\sin\theta - \theta\cos\theta)\ln\tan\tfrac{1}{2}\theta + \cos\theta S(\theta)\right] + c_0\sin\theta + c_1\theta\cos\theta + c_2\cos\theta\,. \tag{79}$$

Applying the three boundary conditions given by Eq. (53) and making use of $S(0) = 0$, the three constants c_0, c_1, and c_2 can be determined. Thus we find

$$c_0 = \alpha\,, \qquad c_2 = 0$$
$$c_1 = \left(\tfrac{1}{2} - 8\alpha\pi^{-2}\right)S\left(\tfrac{1}{2}\pi\right) + 4\alpha\pi^{-2} - \tfrac{1}{2}\,. \tag{80}$$

The first-order solution is, therefore,

$$F_1 = -\frac{2\alpha}{\pi}\theta + \left(\frac{\pi}{4} - \frac{4\alpha}{\pi}\right)\left[(\theta\cos\theta - \sin\theta)\ln\tan\tfrac{1}{2}\theta - \cos\theta S(\theta)\right] + \alpha\sin\theta + \left[\left(\tfrac{1}{2} - 8\alpha\pi^{-2}\right)S\left(\tfrac{1}{2}\pi\right) + 4\alpha\pi^{-2} - \tfrac{1}{2}\right]\theta\cos\theta\,. \tag{81}$$

C. Complete Solution

The first-order corrections appearing in Eq. (81) can be added to the leading-order solution. For added clarity, the resulting function and its derivatives are reproduced below. Written at $O(\varepsilon^2)$, we have

$$F(\theta) = \sin\theta + \varepsilon\left\{-\frac{2\alpha}{\pi}\theta + \left(\frac{\pi}{4} - \frac{4\alpha}{\pi}\right)\left[(\theta\cos\theta - \sin\theta)\ln\tan\tfrac{1}{2}\theta + \cos\theta S(\theta)\right] + \alpha\sin\theta + \left[\left(\tfrac{1}{2} - 8\alpha\pi^{-2}\right)S\left(\tfrac{1}{2}\pi\right) + 4\alpha\pi^{-2} - \tfrac{1}{2}\right]\theta\cos\theta\right\} \tag{82}$$

$$F'(\theta) = \cos\theta + \varepsilon\left\{\frac{2\alpha}{\pi} - \frac{\pi}{4} + \left(\frac{\pi}{4} - \frac{4\alpha}{\pi}\right)\left[\sin\theta S(\theta) - \theta\sin\theta\ln\tan\tfrac{1}{2}\theta\right] + \alpha\cos\theta + \left[\left(\tfrac{1}{2} - 8\alpha\pi^{-2}\right)S\left(\tfrac{1}{2}\pi\right) + 4\alpha\pi^{-2} - \tfrac{1}{2}\right](\cos\theta - \theta\sin\theta)\right\} \tag{83}$$

$$F''(\theta) = -\sin\theta + \varepsilon\left\{\left(\frac{\pi}{4} - \frac{4\alpha}{\pi}\right)\left[\cos\theta S(\theta) - (\sin\theta + \theta\cos\theta)\ln\tan\tfrac{1}{2}\theta\right] - \alpha\sin\theta - \left[\left(\tfrac{1}{2} - 8\alpha\pi^{-2}\right)S\left(\tfrac{1}{2}\pi\right) + 4\alpha\pi^{-2} - \tfrac{1}{2}\right](2\sin\theta + \theta\cos\theta)\right\} \tag{84}$$

$$F'''(\theta) = -\cos\theta + \varepsilon\left\{\left(\frac{\pi}{4} - \frac{4\alpha}{\pi}\right)\left[-\sin\theta S(\theta) - (2\cos\theta - \theta\sin\theta)\ln\tan\tfrac{1}{2}\theta - 1\right] - \alpha\cos\theta - \left[\left(\tfrac{1}{2} - 8\alpha\pi^{-2}\right)S\left(\tfrac{1}{2}\pi\right) + 4\alpha\pi^{-2} - \tfrac{1}{2}\right](3\cos\theta - \theta\sin\theta)\right\}. \tag{85}$$

Note that, following Eq. (52), primes have been used to denote differentiation with respect to θ. When reverting back to y, one must use $F = F(\frac{1}{2}\pi y)$, $F_y = \frac{1}{2}\pi F'(\theta)$, $F_{yy} = \frac{1}{4}\pi^2 F''(\theta)$, etc.

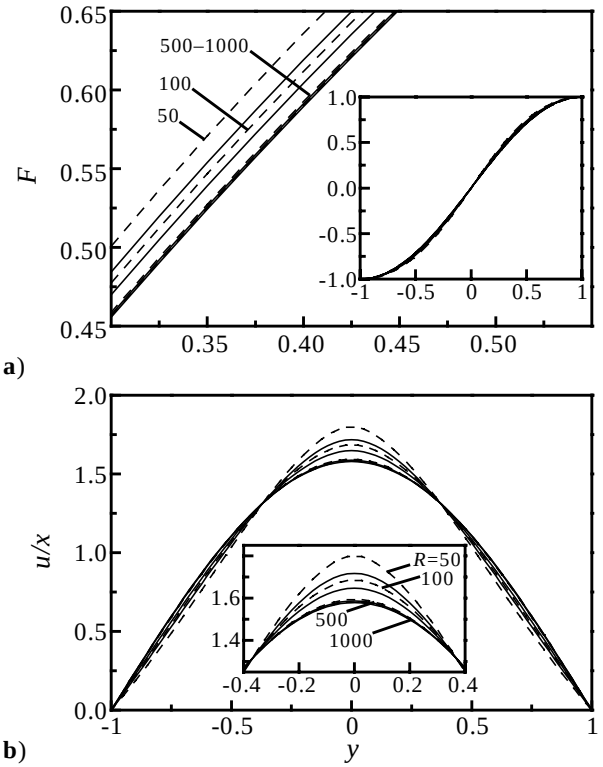

Fig. 2 Comparison between numerical (—) and analytical (- - -) solutions for a) F, and b) u/x at $\alpha = 10$ and $50 \le R \le 1000$.

V. Flow Characterization

From the characteristic function F, all flow ingredients can be evaluated analytically, from the foregoing formulations, and numerically, from a Runge-Kutta solver. Our numerical results use a sufficiently small tolerance to the point of making them accurate in seven significant digits. We thus consider the numerical error to be insignificant.

A. Comparison at Constant Regression Ratio

Using a constant regression ratio of $\alpha = 10$, numerical and analytical solutions for F (or $-v$) and u/x are illustrated in Fig. 2. From Fig. 2a, it may be inferred that Eq. (82) matches the numerical solution quite accurately, especially for $R > 100$. In fact, for $R \geq 500$, results become indistinguishable. Even at a low injection Reynolds number of 50, the analytical solution remains practical. Similar trends are observed in Fig. 2b where the normalized axial velocities are compared. It appears that Eq. (83) is an adequate approximation to the exact solution. As shown, the largest asymptotic error occurs in the vicinity of the core, and for relatively small values of R. These results are reassuring since they indicate an improvement in the accuracy of the analytical expressions at larger values of R. Thus they become ideally suited to model the hard-blowing process in cold-flow experiments or slab rocket motors with large injection Reynolds numbers.

B. Comparison at Constant Reynolds Number

Keeping the Reynolds number fixed at several discrete values (of 100, 500, and 1000), the regression ratio is now varied from $\alpha = 0$ to a large value. Numerical and analytical solutions for u/x are depicted in Fig. 3. Figure 3a indicates that, at a low value of $R = 100$, the solution is more sensitive to the wall regression ratio than at higher Reynolds numbers. In fact, for $R = 1000$, only small differences appear to exist between the $\alpha = 0$ and $\alpha = 100$ case. This justifies ignoring the wall regression rate in high Reynolds number applications. Since a value of R in excess of 1000 is not uncommon in reactive rocket motors, the assumption of a fixed boundary seems reasonable. However, for moderate R, Fig. 3a indicates that noticeable differences due to regression can occur. These need to be carefully accounted for by using, for instance, Eq. (83) in unison with Eq. (39).

It is clear from Fig. 3 that the accuracy of the analytical formulation deteriorates when the Reynolds number is small and the regression ratio is large. This can be explained by referring the reader to the coefficient of the second term in Eq. (48). In that regard, we also recall that the relevant perturbation solution was based implicitly on the condition that

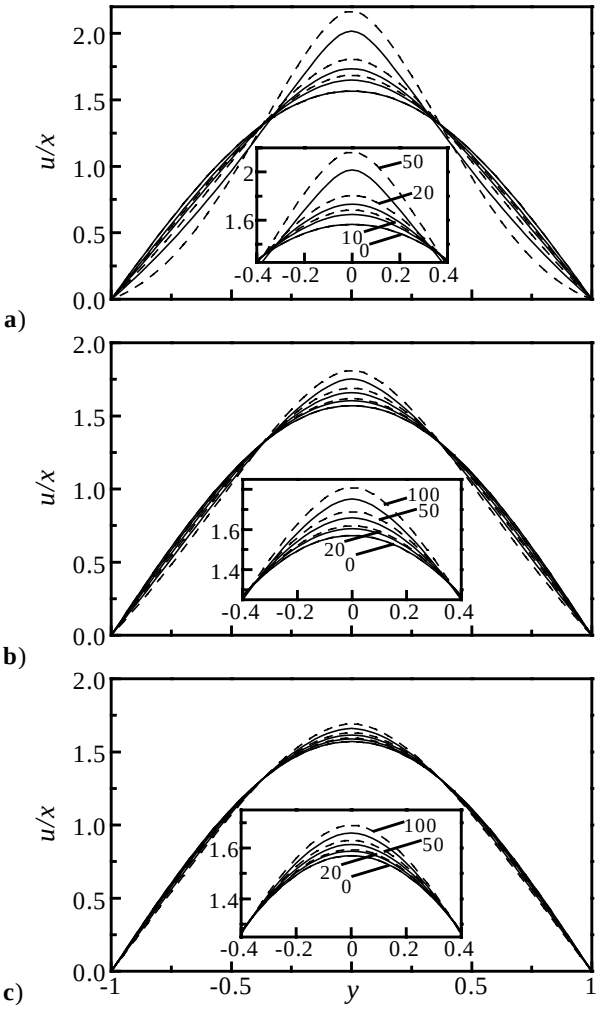

Fig. 3 Comparison between normalized axial velocities obtained from numerical (—) and analytical (- - -) solutions over a range of wall regression rates ($0 \leq \alpha \leq 100$). Here, the injection Reynolds numbers are a) 100, b) 500, and c) 1000.

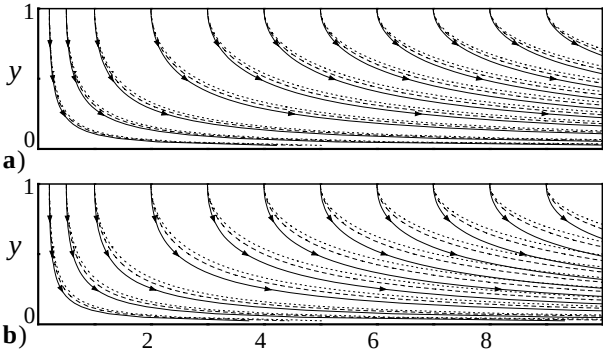

Fig. 4 Comparison between a) numerical and b) analytical streamlines for $\alpha = 10$ and $R = 20$ (—), 50 (- - -), and 1000 (⋯).

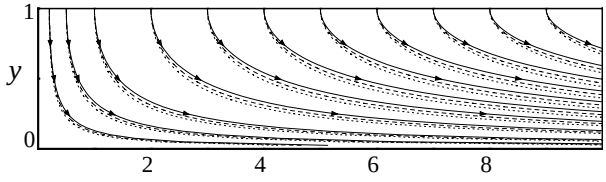

Fig. 5 Mean-flow streamlines for $R = 50$ and $\alpha = 0$ (—), 10 (- - -), and 20 ($\cdots$).

$\alpha\varepsilon \ll 1$. Thus, as long as $\alpha \ll R$, one can expect the solution to be quite accurate. Conversely, as $\alpha \to R$, the analytical formulation is expected to deteriorate. This should not be an alarming issue since, in practical problems, α is seldom larger than 20.

C. Flow Streamlines

In order to better visualize the resulting flow motion, streamlines emanating from several discrete points are shown in Figs. 4 and 5 for several values of R and α. In Fig. 4, increasing the Reynolds number at constant regression rate is seen to increase the flow turning severity. This can be explained by resorting to mass conservation. As mass is injected more rapidly into the chamber, removal of added mass near the head end requires an increasingly larger axial velocity component. Hence, in order to produce the necessary downstream convection, the relative magnitude of the axial versus normal velocity must grow proportionately larger with successive increases in R. As expected from a perturbative standpoint, the agreement between Fig. 4a and Fig. 4b is excellent for $R = 1000$, but deteriorates as R is reduced to 20. An opposite effect is observed when α is varied while holding R constant.

The streamline sensitivity to α is illustrated in Fig. 5. There, it can be observed that the flow turning becomes delayed when the wall regression rate is increased. This can be attributed to the fact that, when the walls expand more rapidly, the ratio of axial to normal mean-flow velocities is diminished. In theory, the reduction in axial velocity can continue until reaching zero. That hypothetical case takes place when the relative fluid velocity at the wall is exactly offset by the speed of the expanding walls. If that condition were to occur, the streamlines would have to be parallel and confined to the neighborhood of the wall.

VI. Other Flow Properties

Having characterized the velocity field, the remaining flow properties, such as pressure and stress distributions, can be now examined.

A. Normal Pressure Distribution

The normal pressure gradient can be obtained by substituting the velocity components of Eq. (23) into Eq. (3). Due to the dependence of the normalized variables on time, one must proceed carefully with the chain derivatives. These include

$$\frac{\partial \overline{v}}{\partial t} = -\frac{\partial}{\partial t}\left(\frac{\nu}{a}\overline{F}\right) = \frac{\nu^2\alpha}{a^3}\left(\overline{F} + y\overline{F}_y\right) \tag{86}$$

$$\frac{\partial \overline{v}}{\partial \overline{x}} = 0\,, \quad \frac{\partial^2 \overline{v}}{\partial \overline{x}^2} = 0 \tag{87}$$

$$\overline{v}\,\frac{\partial \overline{v}}{\partial \overline{y}} = \overline{v}\,\frac{\partial \overline{v}}{\partial y}\frac{\partial y}{\partial \overline{y}} = \frac{\nu^2}{a^3}\overline{F}\overline{F}_y\,, \quad \frac{\partial^2 \overline{v}}{\partial \overline{y}^2} = -\frac{\nu}{a^3}\overline{F}_{yy}\,. \tag{88}$$

Following substitution into Eq. (3), a simple rearrangement yields

$$p_y = -\left[\varepsilon F_{yy} + FF_y + \alpha\varepsilon\left(F + yF_y\right)\right], \tag{89}$$

where

$$p = \frac{\overline{p}}{\rho v_w^2}\,. \tag{90}$$

The normal pressure distribution can now be determined by integrating Eq. (89) while observing the boundary conditions given by Eq. (47). Letting p_c be the pressure at the centerline, one may proceed from

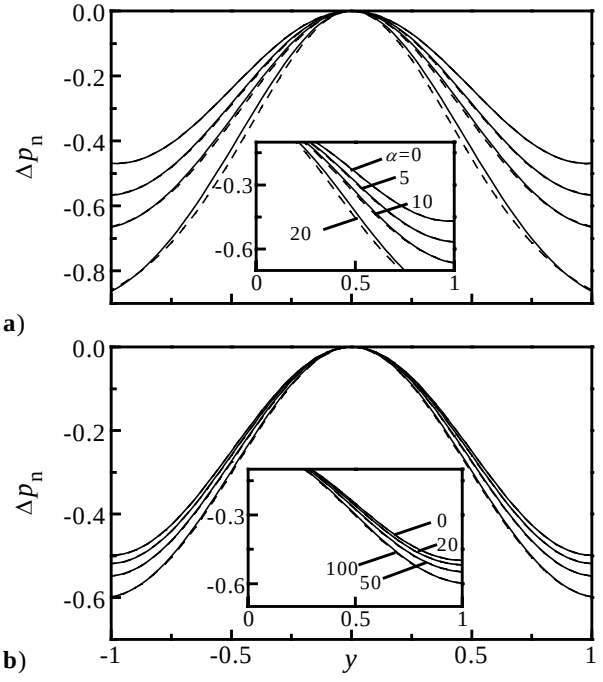

Fig. 6 Comparison between numerical (—) and analytical (- - -) pressure drops in the normal direction for a) $R = 50$, and b) $R = 1000$. Enlargements are shown in the inset.

$$\int_{p_c}^{p(y)} \mathrm{d}p = \int_0^y -\left[\varepsilon F_{yy} + F F_y + \alpha\varepsilon\left(F + yF_y\right)\right]\mathrm{d}y\,. \tag{91}$$

Using $FF_y = \frac{1}{2}(F^2)_y$, and $(F + yF_y) = (yF)_y$, one may integrate Eq. (91) directly into

$$\Delta p_{\mathrm{n}} = \varepsilon F_y(0) - \left(\varepsilon F_y + \tfrac{1}{2}F^2 + \alpha\varepsilon yF\right). \tag{92}$$

Figure 6 below illustrates the pressure distribution for several levels of injection and regression. For every level of injection, the absolute pressure drop is largest near the walls. Increasing the regression ratio also increases the pressure drop. Comparing Fig. 6a to Fig. 6b, the sensitivity of the pressure to variations in wall expansion appears to be less significant at high Reynolds numbers. Due to the uniform agreement between analytic and numeric predictions, the two types can be hardly discerned except for small R and large α (Fig. 6a). Also, for small $\varepsilon\alpha$, the normal pressure gradient is near zero at the wall.

B. Axial Pressure Distribution

Similar substitutions into Eq. (2) give rise to a closed-form expression for the axial pressure gradient. Using

$$\overline{u}_t = \left(\frac{\nu\overline{x}}{a^2}\overline{F}_y\right)_t = \frac{\nu\overline{x}}{a^2}\overline{F}_{yy}\frac{\partial y}{\partial t} - \frac{2\nu\overline{x}\dot{a}}{a^3}\overline{F}_y\,, \tag{93}$$

the pressure gradient can be derived from the axial momentum equation,

$$p_x = x\left[\varepsilon F_{yyy} + F F_{yy} - \left(F_y\right)^2 + \alpha\varepsilon\left(2F_y + yF_{yy}\right)\right]. \tag{94}$$

Equation (94) can, in turn, be integrated to obtain an axial pressure distribution at any spatial location:

$$\Delta p_{\mathrm{a}} = \tfrac{1}{2}x^2\left[\varepsilon F_{yyy} + F F_{yy} - \left(F_y\right)^2 + \alpha\varepsilon\left(2F_y + yF_{yy}\right)\right]. \tag{95}$$

The character of the axial pressure distribution is similar to that of Eq. (92). Namely, small variations are detected for large R.

C. Shear Stress Distribution

Starting with Newton's equation for shear stress,

$$\overline{\tau} = \mu\left(\frac{\partial\overline{v}}{\partial\overline{x}} + \frac{\partial\overline{u}}{\partial\overline{y}}\right), \tag{96}$$

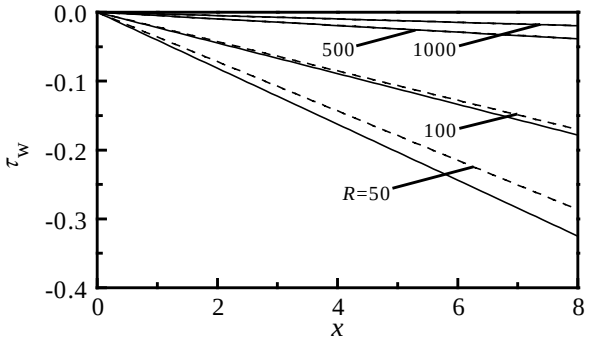

Fig. 7 Comparison between numerical (—) and analytical (- - -) wall shear stresses for $\alpha = 10$ and a range of R.

one may substitute the velocity into Eq. (96) and get

$$\overline{\tau} = \frac{\rho\nu^2\overline{x}}{a^3}\overline{F}_{yy}\,. \tag{97}$$

To be consistent with the pressure, the shear stress may be normalized in a manner to read

$$\tau = \frac{\overline{\tau}}{\rho v_{\mathrm{w}}^2} = \varepsilon x F_{yy}\,. \tag{98}$$

At the wall, the stress becomes

$$\tau_{\mathrm{w}} = \varepsilon x F_{yy}(1)\,. \tag{99}$$

A plot of the wall shear stress is shown in Fig. 7 for a fixed value of α and a range of Reynolds numbers. As the Reynolds number becomes very large, the role of viscosity diminishes, and the shear at the wall becomes less appreciable. As expected, the agreement between asymptotics and numerics also improves with increasing R.

VII. Conclusions

In this article, an exact similarity solution to the Navier-Stokes equations is presented. The problem arises in the context of a fluid entering a porous channel with regressing walls. The similarity transformations in space and time change the momentum equation into a single, nonlinear, differential equation. The resulting equation reduces to the classic Berman equation for a channel with stationary walls. Closed-form solutions obtained using regular perturbations and the method of variation of parameters are shown to coincide with the numerical solution over a useful range of parameters. Due to their adequate accuracy, these explicit formulations are practically equivalent to the exact solution, provided that the ratio of regression and

injection parameters (α / R) is small. When injection is increased, the effect of varying the regression rate becomes less pronounced. Larger values of R also improve the accuracy of the analytical expressions. Their improved accuracy makes them suitable for modeling the hard-blowing process in cold-flow experiments and slab rocket motors. Increasing the Reynolds number is also found to accelerate flow turning and to increase the ratio of axial to normal velocities. Conversely, increasing wall regression seems to inhibit flow turning while diminishing the axial to normal velocity ratio. For Reynolds numbers in excess of 1000, our viscous solution approaches Taylor's inviscid profile, irrespective of the regression rate. This justifies the use of Taylor's profile in modeling the hard-blowing process in rocket motors.

References

[1]Flandro, G. A., "On Flow Turning," AIAA, Paper 95-2530, July, 1995.

[2]Flandro, G. A., "Effects of Vorticity on Rocket Combustion Stability," *Journal of Propulsion and Power,* Vol. 11, No. 4, 1995, pp. 607-625.

[3]Flandro, G. A., "Effects of Vorticity Transport on Axial Acoustic Waves in a Solid Propellant Rocket Chamber," in *Combustion Instabilities Driven by Thermo-Chemical Acoustic Sources, Noise Control & Acoustics* American Society of Mechanical Engineers, New York, 1989, Vol. 4, pp. 53-61.

[4]Majdalani, J., "Vortical and Acoustical Mode Coupling inside a Two-Dimensional Cavity with Transpiring Walls," *Journal of the Acoustical Society of America,* Vol. 106, No. 1, 1999, pp. 46-56.

[5]Majdalani, J., "The Boundary Layer Structure in Cylindrical Rocket Motors," *AIAA Journal,* Vol. 37, No. 4, 1999, pp. 505-508.

[6]Majdalani, J., and Van Moorhem, W. K., "A Multiple-Scales Solution to the Acoustic Boundary Layer in Solid Rocket Motors," *Journal of Propulsion and Power,* Vol. 13, No. 2, 1997, pp. 186-193.

[7]Majdalani, J., and Van Moorhem, W. K., "Improved Time-Dependent Flowfield Solution for Solid Rocket Motors," *AIAA Journal,* Vol. 36, No. 2, 1998, pp. 241-248.

[8]Culick, F. E. C., "Rotational Axisymmetric Mean Flow and Damping of Acoustic Waves in a Solid Propellant Rocket," *AIAA Journal,* Vol. 4, No. 8, 1966, pp. 1462-1464.

[9]Taylor, G. I., "Fluid Flow in Regions Bounded by Porous Surfaces," *Proceedings of the Royal Society, London, Series A,* Vol. 234, No. 1199, 1956, pp. 456-475.

[10]Yuan, S. W., "Further Investigation of Laminar Flow in Channels with Porous Walls," *Journal of Applied Physics,* Vol. 27, No. 3, 1956, pp. 267-269.

[11]Baum, J. D., Levine, J. N., and Lovine, R. L., "Pulsed Instabilities in Rocket Motors: A Comparison between Predictions and Experiments," *Journal of Propulsion Power,* Vol. 4, No. 4, 1988.

[12]Sabnis, J. S., Gibeling, H. J., and McDonald, H., "Navier-Stokes Analysis of Solid Propellant Rocket Motor Internal Flows," *Journal of Propulsion and Power,* Vol. 5, No. 6, 1989, pp. 657-664.

[13]Beddini, R. A., "Injection-Induced Flows in Porous-Walled Ducts," *AIAA Journal,* Vol. 24, No. 11, 1986, pp. 1766-1773.

[14]Dunlap, R., Willoughby, P. G., and Hermsen, R. W., "Flowfield in the Combustion Chamber of a Solid Propellant Rocket Motor," *AIAA Journal,* Vol. 12, No. 10, 1974, pp. 1440-1445.

[15]Dunlap, R., Blackner, A. M., Waugh, R. C., Brown, R. S., and Willoughby, P. G., "Internal Flow Field Studies in a Simulated Cylindrical Port Rocket Chamber," *Journal of Propulsion and Power,* Vol. 6, No. 6, 1990, pp. 690-704.

[16]Dunlap, R., Blackner, A. M., Waugh, R. C., Brown, R. S., and Willoughby, P. G., "Internal Flow Field Studies in a Simulated Cylindrical Port Rocket Chamber," *Journal of Propulsion and Power,* Vol. 8, No. 6, 1992, pp. 1167-1176.

[17]Berman, A. S., "Laminar Flow in Channels with Porous Walls," *Journal of Applied Physics,* Vol. 24, No. 9, 1953, pp. 1232-1235.

[18]Yuan, S. W., and Finkelstein, A. B., "Laminar Pipe Flow with Injection and Suction through a Porous Wall," *Transactions of the American Society of Mechanical Engineers: Journal of Applied Mechanics, Series E,* Vol. 78, 1956, pp. 719-724.

[19]Goto, M., and Uchida, S., "Unsteady Flows in a Semi-Infinite Expanding Pipe with Injection through Wall," *Transactions of the Japan Society for Aeronautical and Space Sciences,* Vol. 33, No. 9, 1990, pp. 14-27.

[20]Coats, D. E., and Dunn, S. S., "Solid Performance Program (SPP) Version 7.2 Vav," SEA TR 95-02, Software and Engineering Associates, Inc., 1995.

[21]Coats, D. E., and Dunn, S. S., "Improved Motor Stability Predictions for 3-D Grains Using the SPP Code," AIAA 33rd Joint Propulsion Conference, Paper 97-33251, July, 1997.

[22]Uchida, S., and Aoki, H., "Unsteady Flows in a Semi-Infinite Contracting or Expanding Pipe," *Journal of Fluid Mechanics,* Vol. 82, No. 2, 1977, pp. 371-387.